Research Article

Darren Yi Sern Low, Camille Keisha Mahendra, Janarthanan Supramaniam, Loh Teng Hern Tan, Learn Han Lee, Sivakumar Manickam, Bey Hing Goh*, Khang Wei Tan*, and Siah Ying Tang*

Ultrasound-enhanced biosynthesis of uniform ZnO nanorice using *Swietenia macrophylla* seed extract and its *in vitro* anticancer activity

https://doi.org/10.1515/ntrev-2021-0044
received March 6, 2021; accepted June 7, 2021

Abstract: In this study, ultrasonically driven biosynthesis of zinc oxide nanoparticles (ZnO NPs) using *Swietenia macrophylla* seed ethyl acetate fraction (SMEAF) has been reported. X-ray powder diffraction (XRD) and Fourier-transform infrared spectroscopy (FTIR) analyses confirmed the presence of a pure hexagonal wurtzite structure of ZnO. Field emission scanning electron microscope images revealed the formation of uniquely identifiable uniform rice-shaped biologically synthesized ZnO_{SMEAF} particles. The particle sizes of the biosynthesized NPs ranged from 262 to 311 nm. The underlying mechanisms for the biosynthesis of ZnO_{SMEAF} under ultrasound have been proposed based on FTIR and XRD results. The anticancer activity of the as-prepared ZnO_{SMEAF} was investigated against HCT-116 human colon cancer cell lines *via* methyl thiazolyl tetrazolium assay. ZnO_{SMEAF} exhibited significant anticancer activity against colon cancer cells with higher potency than ZnO particles prepared using the chemical method and SMEAF alone. Exposure of HCT-116 colon cancer cells to ZnO_{SMEAF} promoted a remarkable reduction in cell viability in all the tested concentrations. This study suggests that green sonochemically induced ZnO NPs using medicinal plant extract could be a potential anticancer agent for biomedical applications.

Keywords: ultrasound, biosynthesis, ZnO, NPs, *Swietenia macrophylla*, anticancer

*** Corresponding author: Bey Hing Goh,** Biofunctional Molecule Exploratory Group, School of Pharmacy, Monash University Malaysia, 47500 Bandar Sunway, Selangor Darul Ehsan, Malaysia; College of Pharmaceutical Sciences, Zhejiang University, 866 Yuhangtang Road, 310058 Hangzhou, China; Health and Well-Being Cluster, Global Asia in the 21st Century (GA21) Platform, Monash University Malaysia, 47500 Bandar Sunway, Selangor Darul Ehsan, Malaysia, e-mail: goh.bey.hing@monash.edu
*** Corresponding author: Khang Wei Tan,** School of Energy and Chemical Engineering, Xiamen University Malaysia, 43900 Sepang, Selangor Darul Ehsan, Malaysia,
e-mail: khangwei.tan@xmu.edu.my
*** Corresponding author: Siah Ying Tang,** Chemical Engineering Discipline, School of Engineering, Monash University Malaysia, 47500 Bandar Sunway, Selangor Darul Ehsan, Malaysia; Advanced Engineering Platform, School of Engineering, Monash University Malaysia, 47500 Bandar Sunway, Selangor Darul Ehsan, Malaysia; Tropical Medicine and Biology Platform, School of Science, Monash University Malaysia, 47500 Bandar Sunway, Selangor Darul Ehsan, Malaysia, e-mail: patrick.tang@monash.edu
Darren Yi Sern Low: School of Energy and Chemical Engineering, Xiamen University Malaysia, 43900 Sepang, Selangor Darul Ehsan, Malaysia; Chemical Engineering Discipline, School of Engineering, Monash University Malaysia, 47500 Bandar Sunway, Selangor Darul Ehsan, Malaysia
Camille Keisha Mahendra: Biofunctional Molecule Exploratory Group, School of Pharmacy, Monash University Malaysia, 47500 Bandar Sunway, Selangor Darul Ehsan, Malaysia
Janarthanan Supramaniam: Chemical Engineering Discipline, School of Engineering, Monash University Malaysia, 47500 Bandar Sunway, Selangor Darul Ehsan, Malaysia
Loh Teng Hern Tan: Clinical School Johor Bahru, Jeffrey Cheah School of Medicine and Health Sciences, Monash University Malaysia, 80100 Johor Bahru, Johor Darul Ta'zim, Malaysia; Novel Bacteria and Drug Discovery Research Group, Microbiome and Bioresource Research Strength, Jeffrey Cheah School of Medicine and Health Sciences, Monash University Malaysia, 47500 Bandar Sunway, Selangor Darul Ehsan, Malaysia
Learn Han Lee: Novel Bacteria and Drug Discovery Research Group, Microbiome and Bioresource Research Strength, Jeffrey Cheah School of Medicine and Health Sciences, Monash University Malaysia, 47500 Bandar Sunway, Selangor Darul Ehsan, Malaysia
Sivakumar Manickam: Petroleum and Chemical Engineering Department, Faculty of Engineering, Universiti Teknologi Brunei, BE1410 Bandar Seri Begawan, Brunei Darussalam

1 Introduction

Research in nanotechnology is ever-growing and synergistic with the global advancements in science, technology, and engineering. Coincidentally, materials in the nanoscale have proven to improve the quality of life of global inhabitants in various ways due to their novel properties, which arise from their morphology, distribution, and size [1]. Applications of nanomaterials have been widely demonstrated in the fields of civil engineering [2], biomedicine [3], food packaging [4], as well as in the generation of smart materials [5].

In the category of metallic oxide nanoparticles commonly used in the semiconductor and electronics industry, zinc oxide (ZnO) has been recently studied in-depth, and its potential is explored in biological, pharmaceutical, and environmental applications [6,7]. It could also be extended further to advanced technologies such as chemical gas sensing, flexible conductors, self-cleaning materials, and long-term dual-protective cosmeceuticals against UV-A and UV-B radiation [8]. Some advantages of ZnO nanoparticles include antifungal, anticancer, and antibacterial properties, high chemical stability, long shelf-life, high thermal resistance, and low cost [8–10]. Studies on ZnO are also highly supported from a human safety standpoint as it is "generally recognized as safe" by the Food and Drug Administration, USA [11].

Previously, research has been conducted to completely reduce the scale of particles and evaluate the novel properties of these nanoparticles. With the ever-increasing demand for nanomaterials, there is a need for a "greener," cleaner, and more sustainable route of synthesis to reduce their environmental footprint. Currently, the concepts of green chemistry and green synthesis are becoming more popular. It is a more sustainable and eco-friendly method of nanomaterial synthesis which uses less or nonhazardous materials from renewable resources such as plants and microorganisms [12]. Plant sources are rich in secondary metabolites (phytochemicals) such as terpenoids, flavonoids, alkaloids, phenols, and steroids [13,14]. These phytochemicals possess therapeutic characteristics which add value to the nanoparticles synthesized from a biomedical perspective. For instance, various parts of plants such as fruits, flowers, seeds, stems, barks, and roots have been tested for their capabilities to synthesize nanomaterials with various value-added pharmaceutical properties. Reviews by Bandeira *et al.* [15] and Kalpana and Rajeshwari [16] highlighted numerous biological species such as plants, seaweeds, and microbes, aiding the green synthesis of ZnO NPs and were then applied in biomedicine based on their properties. Furthermore, Ranjbar *et al.* [17] showed that biosynthesized ZnO NPs using *Mentha mozaffarianni* plant extract were effective against human cervical, breast, and colon cancer cells without significant side effects on healthy cells.

Nowadays, ultrasound is common to nebulize solutions into ultrafine mixtures, synthesizing nanoparticles as well as dispersing them to improve homogeneity [18,19]. Briefly, ultrasonic technology involves using acoustic waves with a frequency of approximately 20 to 25 kHz and up to 1,000 kHz, which interact with the particles [20]. Ultrasonics and sonochemistry are based on the continuous cycles of formation, growth, and collapse of microbubbles in a solution that causes structural disruptions and modifications [21,22]. The collapse of these microbubbles generates localized energy hotspots with temperatures up to 10,000 K and pressures up to 1,000 bar [23]. Consequently, these conditions disrupt weak non-covalent bonds, causing morphological changes, and disintegrating large colloidal aggregates. Ultrasonic waves could be induced using different equipment. One of which is using a cylindrical probe (horn) which is immersed into the working solution. Another is a novel high-intensity ultrasonic tubular reactor where the waves are emitted radially and are considered for working solutions of larger volumes [21]. An extensive review by Wojnarowicz *et al.* [8] explains the widespread use of microwave and acoustic cavitation-assisted technologies to synthesize tailored ZnO nanomaterials and fulfill the eco-friendly approach criterion. Bayrami *et al.* [24] used ultrasonic treatment to aid the biosynthesis of ZnO NPs using the leaf extract of *Vaccinium arctostaphylos* and assessed its antidiabetic, antibacterial, and oxidative activities. They also synthesized enriched ZnO NPs for antidiabetic and antibacterial applications using *Nasturtium officinale* leaf extract through combined microwave and ultrasound methods [25]. These studies show the versatility and compatibility of ZnO NPs synthesis methods with various natural extracts to enhance pre-existing biological properties.

Swietenia macrophylla (*S. macrophylla*) also known as the big-leaved mahogany tree belongs to the Meliaceae family and is widely found in Asia and tropical and subtropical regions. *S. macrophylla* is an important indigenous medicinal plant in Malaysia with potential anticancer, anti-inflammatory, and antitumor properties [26–28]. The fruit of this tree was termed as "sky fruit" due to its growth against gravity [29]. Many phytochemicals consisting of limonoids could be extracted from different parts of *S. macrophylla* such as the seeds, leaves, and branches, and have been attributed to the bioactivities exhibited by this plant [29]. Some of the identified compounds include swietenine, swietemahonin E, 3-*O*-tigloyl-6-*O*-acetylswietenolide, and

3,6-*O,O*-diacetylswietenolide [30]. The ethyl acetate fraction of the seeds of *S. macrophylla* (SMEAF) was shown to induce reactive oxygen species (ROS) production in cancer cells, leading to the activation of apoptosis through the p53 tumor-suppressing proteins [31,32]. Although many different plant species had been used in the biological synthesis of ZnO NPs, no research regarding its synthesis with the use of SMEAF had been previously reported. Yet, as SMEAF has great potential in its anticancer properties, it was hoped that the aid of SMEAF in ZnO NP synthesis would further enhance its anticancer efficacy at lower concentrations. This increase in SMEAF potency would be beneficial toward future potential users as the dosage would be significantly reduced without compromising its performance in inducing cancer cell death. In addition, the biological synthesis of ZnO NPs could potentially enhance the delivery of SMEAF to cancer cell lines, as compared to SMEAF independently.

In this study, highly uniform ZnO nanorice was synthesized using a greener route with the aid of SMEAF and ultrasonic treatment. As a part of the synthesis process, SMEAF was obtained from the crude extracts of the seeds of *S. macrophylla* through solvent partitioning extraction methods. The bioextract as a stabilizing agent was added during the synthesis of ZnO NPs and was assisted with ultrasonic nebulization. The stabilization and attachment behavior of SMEAF on the synthesized nanoparticles were observed. Preliminary qualitative phytochemical screening was conducted to determine the bioactive substances in SMEAF. Both the neat samples of ZnO NPs (ZnO_{Chem}) and samples synthesized with SMEAF (ZnO_{SMEAF}) were characterized. Particle size (DLS), morphology (FESEM and STEM), and chemical properties (FTIR, EDX, and XRD) were also investigated. Additionally, SMEAF, ZnO_{Chem}, and ZnO_{SMEAF} were subjected to anticancer assessments to evaluate their efficacy against HCT-116 colon cancer cells at different concentrations.

2 Materials and methods

2.1 Materials

Reagents of analytical grade were utilized without any further purification steps. Zinc nitrate hexahydrate ($Zn(NO_3)_2{\cdot}6H_2O$, 99% AR Grade) was purchased from Friendemann Schmidt Chemical Company (US). Sodium hydroxide pellets were obtained from Sigma-Aldrich (Malaysia). 95% technical grade ethanol was procured from Gouden Sdn. Bhd. (Malaysia). HCT-116 cell lines were gifted by Dr. Goh Bey Hing (School of Pharmacy, Monash University). RPMI-1640, fetal bovine serum (FBS), TrypLE Express, and 100× antibiotic–antimycotic were obtained from Gibco (USA). Phosphate buffered saline pellets, trypan blue, 3-(4,5-dimethylthiazol-2-y1)-2,5-diphenyltetrazolium bromide (MTT) reagent, and dimethyl sulfoxide (DMSO) were purchased from Sigma-Aldrich (USA). Cell culture plasticware such as 96-cell culture plates (NEST, USA), 15 mL and 50 mL falcon tubes NEST (USA), serological pipettes (Jet Biofil, China), and pipette tips (Axygen, USA) were also purchased. Other subsidiary chemicals not involved in the main synthesis or tests were included for plant-based phytochemical screening and were used as received.

2.2 Synthesis of ZnO NPs from bioresource

2.2.1 Preparation of seed extract fraction

The dried seeds (600 g) of *S. macrophylla* were acquired from a local market in Selangor, Malaysia. The voucher specimen of the seeds (No. KLU46901) was deposited at the Herbarium of the Institute of Biological Sciences, Faculty of Science, University of Malaya, Malaysia. First, the seeds were dried and then ground finely before soaking in 2.4 L ethanol at room temperature for 72 h. The extract was then filtered from the residue using filter papers and subsequently evaporated at 40°C using a rotary vacuum evaporator to produce a dark yellow crude ethanolic extract. The crude extract was then further fractionated using 800 mL hexane to produce a hexane-soluble solution and hexane-insoluble residues. The remaining hexane-insoluble residue was further separated using 1:1 ratio solvent–solvent portioning of ethyl acetate (600 mL) and water (600 mL). The ethyl acetate fraction was later evaporated *via* rotary vacuum evaporation to obtain SMEAF.

2.2.2 Plant-based phytochemical screening analysis

Phytochemical screening is a qualitative analysis to identify medicinally active or bioactive substances found in naturally occurring species. This screening test was conducted for SMEAF. The method and reagents used in each test are presented in Table 1. As SMEAF is insoluble in water, a control was prepared where ethanol was used to dissolve SMEAF. The quantity of reagents used for the test

is presented in terms of mass ratio. The tests are qualitative and result in either a positive or negative response.

2.2.3 Synthesis of ZnO NPs (ZnO_{Chem})

About 0.38 g $Zn(NO_3)_2{\cdot}6H_2O$ was dissolved in 20 mL distilled water under gentle magnetic stirring until it dissolved completely. The pH of the solution (5.6) was adjusted to 10, using 0.5 M NaOH under constant monitoring using a pH meter. The cloudy mixture was then ultrasonicated using an ultrasound horn (20 kHz, 100 W; NexTgen ultrasonic platform, Sinaptec, France) for five cycles of 15 s each with a 12 s break at 45 W in a water bath. The mixture was then heated to 85°C under gentle stirring for 1 h. A white precipitate was observed until this stage. The mixture was then centrifuged for 5 min at 7,000 rpm. Two wash cycles were carried out on the samples using distilled water. The solvents were removed and left to dry overnight in an aerated oven at 60°C. The dried samples were ground using a mortar and pestle before subjected to characterization.

2.2.4 Synthesis of ZnO NPs with SMEAF (ZnO_{SMEAF})

Similar to the chemical route of synthesis, 0.38 g Zn $(NO_3)_2{\cdot}6H_2O$ was dissolved in 20 mL distilled water under gentle magnetic stirring until it dissolved fully. Separately, 0.20 g SMEAF was dissolved in 10 mL ethanol under magnetic stirring until it dissolved completely. The extract was then poured into $Zn(NO_3)_2{\cdot}6H_2O$ solution under magnetic stirring for 10 min (step 1). The mixture was then ultrasonicated using the horn for five cycles of 15 s each with a 12 s break at 45 W in a water bath (step 2). Subsequently, the pH of the solution was adjusted to 10 using 0.5 M NaOH and then ultrasonicated again under the same settings as above (steps 3 and 4). The mixture was then heated to 85°C under gentle stirring for 1 h (step 5) and centrifuged for 5 min at 7,000 rpm (step 6). Two wash cycles were carried out on the samples using distilled water. The solvents were removed and left to dry overnight in the oven at 60°C (step 7) and ground using a mortar and pestle (step 8) before subjected to further characterization. The resultant powder has a pale-yellow appearance. The schematic flow diagram of the synthesis process and the impact of cavitation on the formation of ZnO_{SMEAF} are depicted in Figure 1.

2.3 Characterization of nanoparticles

Preliminary size measurements of the nanoparticles *via* dynamic light scattering (DLS) were conducted using the Malvern Panalytical Zetasizer ZSP (Malvern Instruments, UK).

Table 1: Qualitative phytochemical screening for SMEAF

Phytoconstituent	Test	Method	Expected observation
Flavonoids	Zn test	Zn dust is added to a mixture of extract and concentrated HCl (1:2)	Dark brown coloration
Phenols	$FeCl_3$ test	Five drops of alcoholic $FeCl_3$ solution are added to the extract (1:1)	Blue-green precipitate
Phlobatannins	Precipitate test	Dilute HCl is added to the extract (1:1) and heated in a water bath at 60°C for 10 min	Red precipitate
Steroids and terpenoids	Salkowski's test	Chloroform and concentrated H_2SO_4 are added to the extract (1:1:2)	Red/brown layer in the lower chloroform interphase
Glycosides	Keller–Kiliani test	Glacial acetic acid, $FeCl_3$ solution, and concentrated H_2SO_4 are added to the extract (1:1:0.5:1)	Brown-ring at the interphase
Amino acids	Ninhydrin test	Ninhydrin is added to acetone (1:5) to form a ninhydrin solution. This solution is added dropwise to the extract	Purple coloration
Fixed oils	Saponification test	Alcoholic KOH is added to the extract (1:1), with drops of phenolphthalein and heated in a water bath at 60°C for 2 h	Formation of soap bubbles
Saponins	Froth test	Distilled water is added to the extract (2:1)	Formation of a stable froth layer
Alkaloids	Wagner's test	Iodine and KI powders are added to distilled water (1:2:15) to form Wagner's reagent. This reagent is added dropwise to the extract	Red-brown precipitate

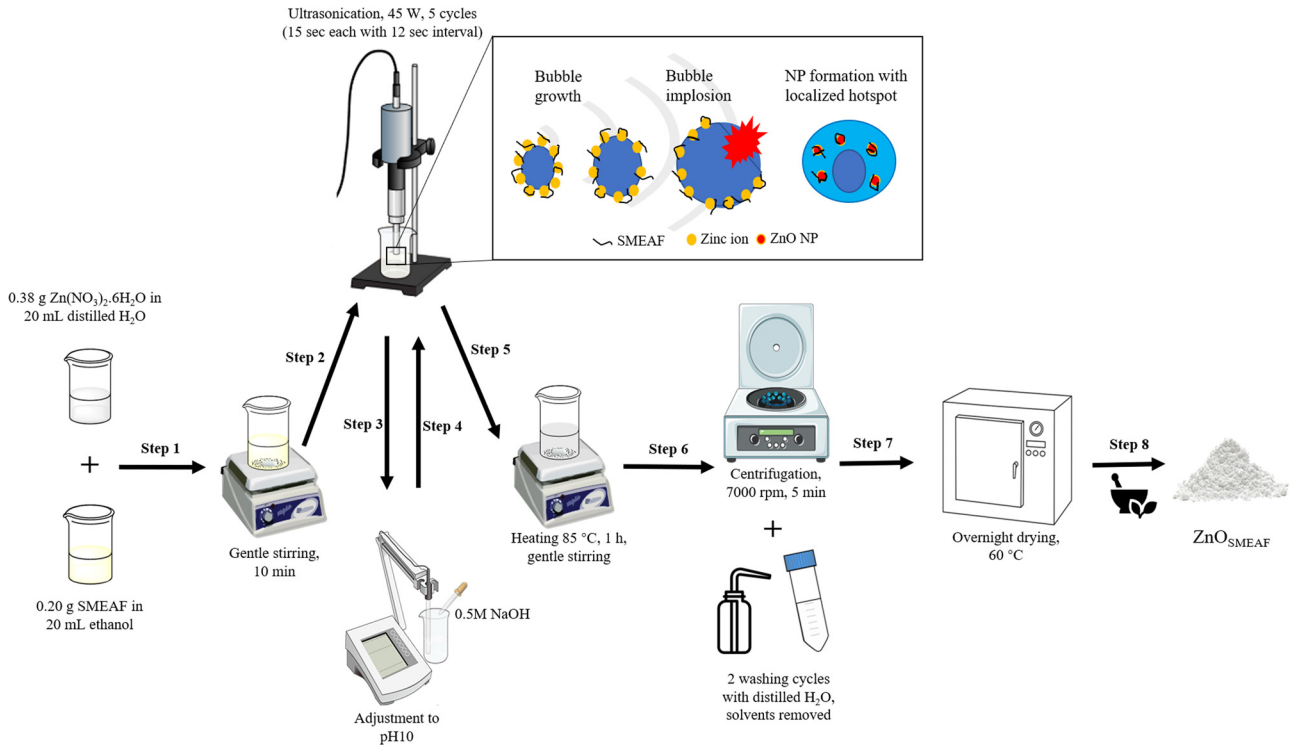

Figure 1: Schematic of the synthesis and the influence of ultrasound on the formation of ZnO_{SMEAF} (inset).

The samples were dispersed in ultrapure water at 1 mg/mL, and the measurements were performed at 25°C. The degree of crystallinity of the nanoparticles was measured via XRD using the Bruker D8 Discover X-ray powder diffractometer (Germany) equipped with Cu Kα (λ = 0.15406 nm) radiation. The scan was obtained using 40 kV and 40 mA at a scanning rate of 0.02° per sec from 10° to 80°. The crystalline size was computed using the Debye–Scherrer's equation, $D = (k\lambda)/(\beta \cos\theta)$, where D is the crystallite size, k is the Scherrer's constant (0.94) [14], λ is the X-ray wavelength, β is the full width at half maxima, and θ is Bragg's angle. Fourier-transform infrared spectroscopy (FTIR) analysis was conducted using the Thermo Scientific Nicolet iS10 Spectrometer (US) to examine the major functional groups in the synthesized nanoparticles. The surface morphologies of the nanoparticles were observed under a Hitachi SU8010 field emission scanning electron microscope (FESEM) (Japan), which was also equipped with an energy dispersive X-ray (EDX) spectrometer (Oxford-Horiba Inca XMax50, Oxford Instruments Analytical, England) for elemental analysis. The same FESEM equipment was switched into TE mode to conduct scanning transmission electron microscopy (STEM) analysis.

2.4 Evaluation of cytotoxicity

2.4.1 Cell culture

HCT-116 human colon cancer cells were maintained in RPMI media supplemented with 10% heat-inactivated (56°C for 30 min) FBS and 1% 100× antibiotic–antimycotic (100 U/mL penicillin, 100 µg/mL streptomycin, and 25 µg/mL amphotericin B) (Gibco, USA). The cells were also kept in a humidified incubator at 37°C with 5% CO_2 and were passaged when confluency reaches 70% using TrypLE Express (Gibco, USA).

2.4.2 Cell treatment and evaluation of cell viability using methyl thiazolyl tetrazolium (MTT) assay

Cell viability was measured using MTT assay as described by Goh and Kadir [32] with some modifications. Briefly, HCT-116 cells were seeded into 96 flat-bottom well plates at a density of 3,000 cells per well. After 24 h, the cells were treated with SMEAF, ZnO_{Chem}, and ZnO_{SMEAF}, at the concentrations as given in Table 2 following their proportions, with cell culture media containing 0.5% (v/v) DMSO as the

Table 2: Concentrations of SMEAF, ZnO_{Chem}, and ZnO_{SMEAF} in the cytotoxic studies against HCT-116

Run	Concentration (μg/mL)*		
	SMEAF (34.6%)	**ZnO_{Chem} (65.4%)**	**ZnO_{SMEAF} (100%)**
1	1.081	2.044	3.125
2	2.163	4.088	6.25
3	4.325	8.175	12.5

*Percentages presented are the proportions of SMEAF and ZnO_{Chem} within ZnO_{SMEAF}. Thus, in this experiment, the concentration of ZnO_{SMEAF} per run does equate to the individual concentrations of SMEAF and ZnO_{Chem}, according to their proportions.

vehicle. The untreated cells (negative controls) were treated with cell culture media containing 0.5% (v/v) DMSO. The cells were then incubated at 37°C with 5% CO_2 for 72 h before analyzing their cell viability. Then, 40 μL 5 mg/mL MTT reagent (Sigma, USA) was added to each well, and the cells were further incubated at 37°C for 4 h before the media was aspirated, and the crystals were dissolved in 100 μL DMSO. The absorbance was measured using a microplate reader (Bio-Tek, USA) at 570 nm. The percentage cell viability was calculated using equation (1), after normalizing all the samples against the untreated cells.

$$\text{Cell viability (\%)} = \frac{\text{Absorbance value of the treated cells}}{\text{Absorbance value of the untreated cells}} \times 100\% \quad (1)$$

2.5 Statistical analysis

All cytotoxic treatment data on HCT-116 cell lines were analyzed for significant difference between groups with one-way analysis of variance and Tukey HSD *post hoc* test using Statistical Package for Social Science version 24.0. The significance value was set at $p \leq 0.05$, and the data were expressed as mean values ± standard deviation.

3 Results and discussion

3.1 Plant-based phytochemical screening analysis

Other than the common parts of the plants (*i.e.*, leaves and roots), which are typically exploited for their properties, seeds also demonstrate significant bioactivities owing to their phytoconstituents [33,34]. The plant extracts show great potential as capping and stabilizing agents due to the presence of a plethora of biocomponents such as phenols, flavonoids, steroids, saponins, and alkaloids [35]. Generally, flavonoids have been widely reported to provide chemical stability to metal oxide nanoparticles and could serve as reducing agents [12,15,36]. In this context, the existence of OH– groups in flavonoids could be dually responsible for reducing zinc precursors into ZnO NPs and exhibiting size control through their capping ability [14,37,38]. The collection of phytoconstituents or secondary metabolites is common in various medicinal plants but could vary depending on the species and their place of origin. Table 3 presents the results of the phytochemical screening tests with corresponding expected observations for a positive outcome.

3.2 Characteristics of the synthesized nanoparticles

The preliminary size analysis was conducted on the as-synthesized nanoparticles using the Zetasizer through the DLS technique for colloids. It could be seen from Figure 2(a) that the size of ZnO_{Chem} is slightly smaller, with a mean of 262 nm and a polydispersity index (PDI) of 0.166. Figure 2(b) exhibits the particle size distribution for ZnO_{SMEAF}, which shows a peak with a mean size of 311 nm and a PDI of 0.402. The addition of the plant extract has increased the particle size. This may contribute to the amalgamation of smaller neighboring particles to form larger nanoparticles, as further biological reduction of the zinc ions occurs [39].

Figure 3 shows the XRD patterns of the as-prepared SMEAF, ZnO_{Chem}, and ZnO_{SMEAF} samples. The peaks within the spectra for both the synthesized samples show crystalline structures corresponding to the hexagonal wurtzite phase of ZnO NPs without any impurities. The observed peaks at the diffraction angles of 31.7°, 34.4°, 36.2°, 47.7°, 56.5°, 62.8°, 66.3°, 67.9°, and 69.2° correspond to the plane facets of 101, 002, 101, 102, 110, 103, 200, 112, and 201, respectively. These correlations are made following the Joint Committee on Powder Diffraction Standards (JCPDS No. 36-3411) for ZnO. The crystalline size for the most prominent peak at the plane facet (101) was computed using Debye–Scherrer's equation. The average crystallite size was found in the range of 26 to 30 nm for both ZnO_{Chem} and ZnO_{SMEAF}, comparable to the findings obtained by Bayrami *et al.* [24].

Table 3: Qualitative plant-based phytochemical screening test results for SMEAF

Phytoconstituent	Test	Expected observation	Outcome
Flavonoids	Zn test	Dark brown coloration	Positive (+)
Phenols	$FeCl_3$ test	Blue-green precipitate	Negative (−)
Phlobatannins	Precipitate test	Red precipitate	Negative (−)
Steroids and terpenoids	Salkowski's test	Red/brown layer in the lower chloroform interphase	Positive (+)
Glycosides	Keller–Kiliani test	Brown-ring at the interphase	Positive (+)
Amino acids	Ninhydrin test	Purple coloration	Negative (−)
Fixed oils	Saponification test	Formation of soap bubbles	Positive (+)
Saponins	Froth test	Formation of a stable froth layer	Positive (+)
Alkaloids	Wagner's test	Red-brown precipitate	Positive (+)

Figure 4 shows the FTIR spectra of the obtained samples. A wide peak observed between 3,650 and 3,250 cm^{-1} for SMEAF and ZnO_{SMEAF} is due to the O–H stretching vibrations that form hydrogen bonds from the organic sample [40]. The peak at 2,927 cm^{-1} from both SMEAF and ZnO_{SMEAF} corresponds to the asymmetrical stretching of C–H bonds or alkyl compounds. Another small peak at 2,853 cm^{-1} from both these samples is linked to the symmetric stretching vibration of C–H bonds of lipid compounds [41]. ZnO_{SMEAF} and ZnO_{Chem} spectra exhibit a small common peak at 2,360 cm^{-1}, possibly due to the absorption of CO_2. A prominent peak from SMEAF and ZnO_{SMEAF} at 1,727 cm^{-1} corresponds to the C=O stretching vibrations, indicating the presence of the ester carbonyl group. Furthermore, the common peak at 1,436 cm^{-1} indicates C–H deformation vibrations of the possible methyl ester group. The peak at 1,222 cm^{-1} shows C–O and COOH stretching vibrations of the aromatic compounds [42]. A clear peak at 882 cm^{-1} between ZnO_{SMEAF} and ZnO_{Chem} demonstrates the stretching vibrations of C–N amine groups [43]. Peaks for SMEAF appearing between 700 and 900 cm^{-1} could be ascribed to C–H bending vibrations, indicating that the extract contains long carbon chains ($^{n}C > 4$) [44].

The electron micrographs (Figure 5(a)–(f)) show the surface morphology of ZnO_{Chem} and ZnO_{SMEAF} samples. From Figure 5(a)–(c), it can be observed that ZnO_{Chem} samples exhibit short nanorice structures. ZnO_{SMEAF} images, as shown in Figure 5(d)–(f), exhibit that the nanorice morphologies remain even with the addition of SMEAF, indicating the effective shape control of the bioextract on the ZnO NPs. This hypothesis is further supported by the STEM images, as indicated in Figure 5(g) and (h), which show consistency in the nanorice shape of ZnO_{SMEAF}. Furthermore, the particles observed through STEM are coherent with the size distribution results obtained through DLS in Figure 2 (262 and 311 nm) for ZnO_{Chem} and ZnO_{SMEAF}, respectively, which follows a normal distribution curve.

Based on the results obtained from characterization, the following mechanism has been proposed for the green synthesis of ZnO_{SMEAF}. Plant extracts containing various phytochemicals such as terpenoids and flavonoids play an important role in reducing the zinc ions and providing stability [39]. As confirmed in the FTIR analysis, the phytochemicals in SMEAF were previously determined to have free O–H and COOH functional groups. The latter is present in ZnO_{SMEAF} but absent in ZnO_{Chem}. These groups would react with ionized zinc aqua complexes to form zinc–phytochemical complexes, as depicted in Figure 6. This was followed by active bioreduction of the complexes to ZnO_{SMEAF} at elevated

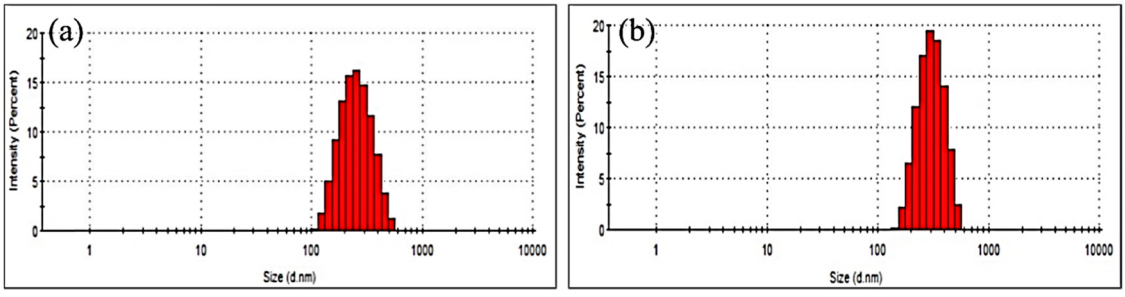

Figure 2: Particle size distribution of (a) ZnO_{Chem} and (b) ZnO_{SMEAF}.

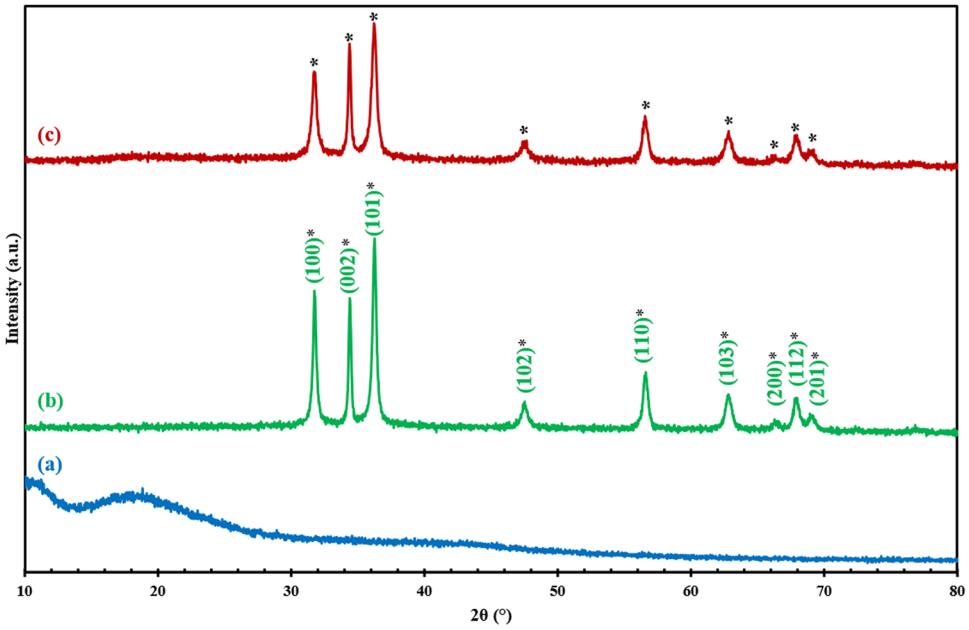

Figure 3: XRD diffractograms of (a) SMEAF, (b) ZnO_{Chem}, and (c) ZnO_{SMEAF}.

temperatures. During the synthesis process, the phytochemicals of SMEAF also act as capping agents to provide stability and prevent overgrowth of the formed ZnO_{SMEAF} [38,42].

The zinc ions were encapsulated by the organic covering of SMEAF, as evident in the TEM micrographs. There was a temporal activation period at the initial stage, where zinc ions would be converted from their divalent oxidation state to their zero valent state, and nucleation of the reduced zinc occurs [45]. Subsequently, a period of particle growth would follow, where smaller zinc particles would agglomerate together to achieve stability, as more zinc ions are being biologically reduced. As the growth of ZnO_{SMEAF} continues, these particles would agglomerate to form unique morphologies, *i.e.*, rice-shaped particles. In the termination phase, the ability of SMEAF to stabilize and cap ZnO_{SMEAF} ultimately determines its most stable form. From a chemical standpoint, equation (2) shows the first degree of formation involving a double exchange of the zinc nitrate precursor and NaOH, forming zinc hydroxide and sodium nitrate as the by-product. Equation (3) shows the secondary

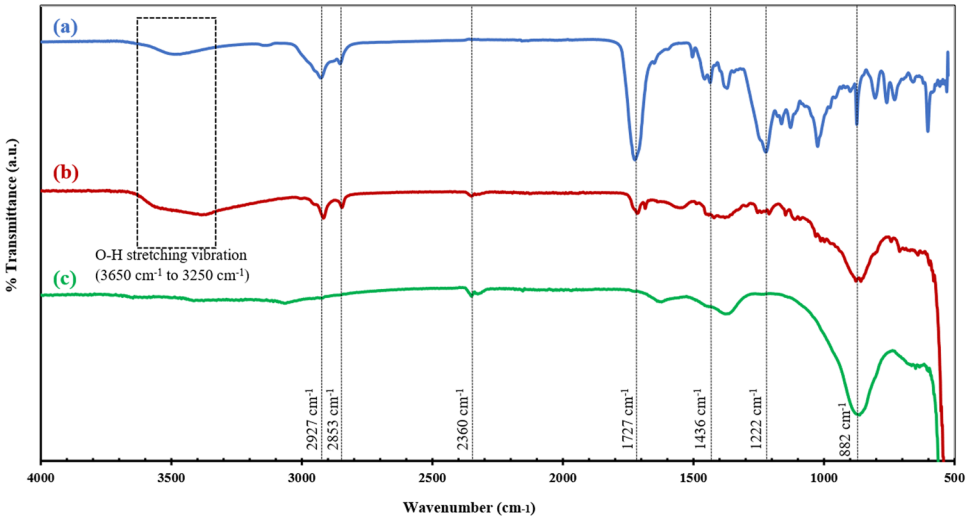

Figure 4: FTIR spectra of (a) SMEAF, (b) ZnO_{SMEAF}, and (c) ZnO_{Chem}.

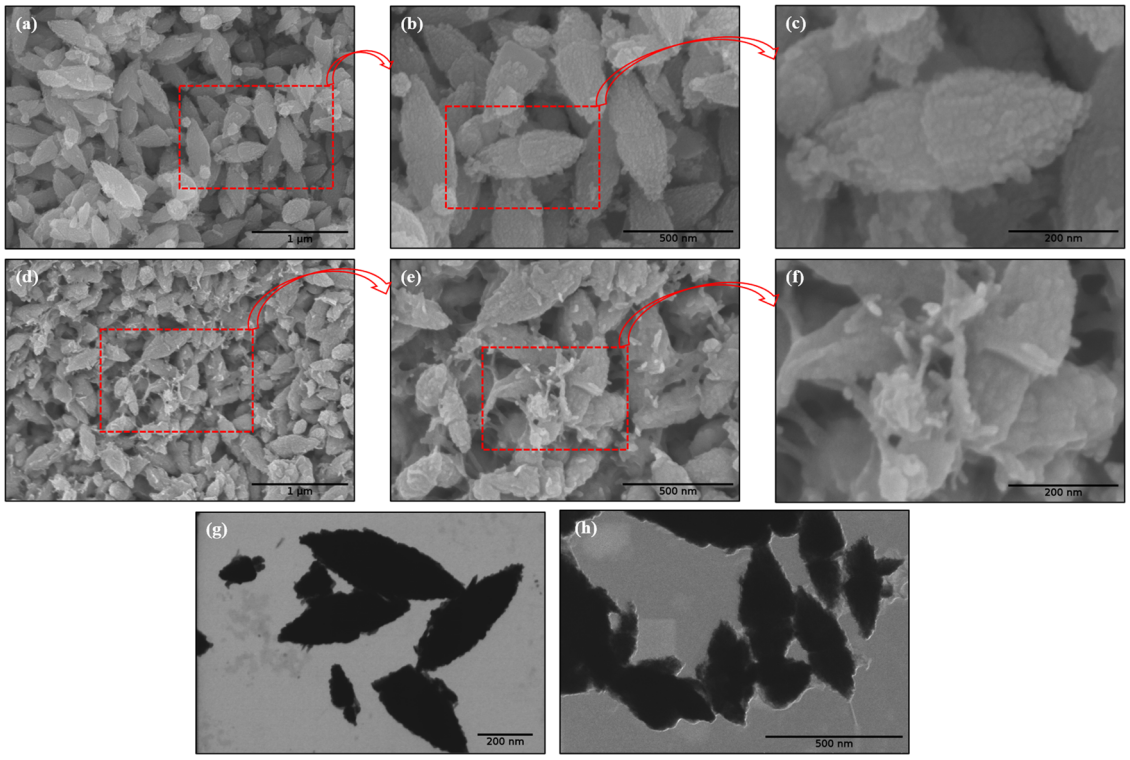

Figure 5: FESEM micrographs of [(a)–(c)] ZnO_{Chem}, [(d)–(f)] ZnO_{SMEAF}; STEM micrographs of (g) ZnO_{Chem}, (h) ZnO_{SMEAF}.

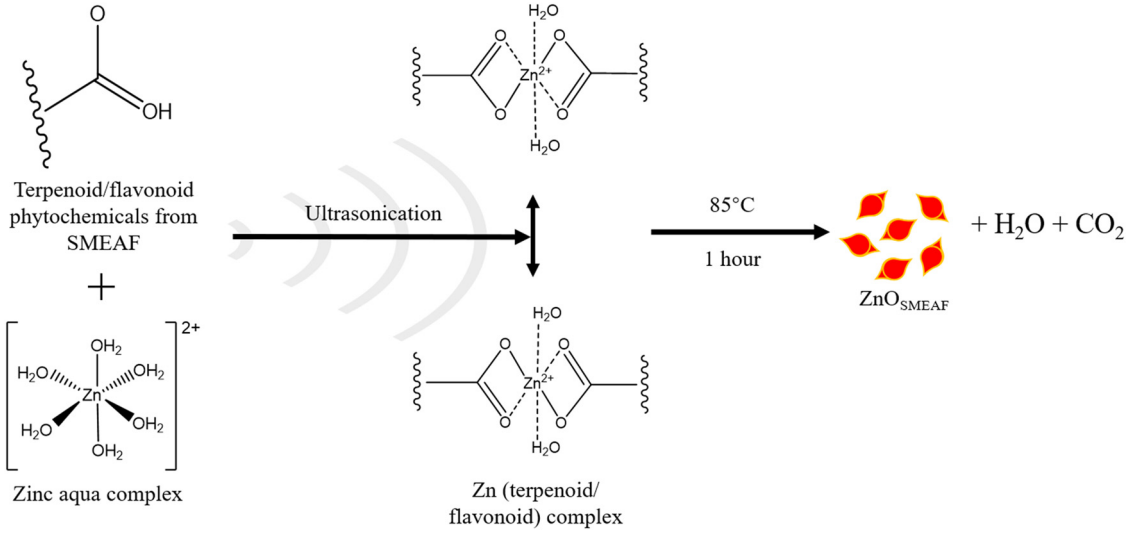

Figure 6: Proposed mechanism for the ultrasonic-aided synthesis of ZnO_{SMEAF}.

decomposition reaction of zinc hydroxide to ZnO_{SMEAF} upon dehydration at elevated temperatures.

$$Zn(NO_3)_2 \cdot 6H_2O + 2NaOH \xrightarrow{\Delta} Zn(OH)_2 + 2NaNO_3 \quad (2)$$

$$Zn(OH)_2 + NaNO_3 \xrightarrow{SMEAF,\Delta} ZnO_{SMEAF} \quad (3)$$

EDX analysis was conducted to confirm the elements present in the samples, and the spectra, as shown in Figure 7, exhibit the elemental distribution by weight (inset). The spectra illustrate that the main constituents in the samples are zinc and oxygen, for both chemical and biological synthesis methods. In addition to Zn and O

elemental peaks, the presence of C was also detected in both methods, but greater in weight percentage for ZnO_{SMEAF}. This could be due to a strong link formed between SMEAF and the ZnO NPs even after several washing cycles during the synthesis. Similar trends were observed by Bayrami *et al.* [24], and in their study, a rise in the weight percentage of C was noted after including bioextracts. No other elements were detected from this analysis, indicating that the samples were produced without impurities.

3.3 ZnO_{Chem} and ZnO_{SMEAF}-induced dose-dependent cytotoxicity

The application of ZnO NPs in cancer treatment is advantageous as these nanoparticles possess inherent cytotoxicity against cancerous cells *in vitro* [46,47]. Endocytosis of NPs is a prerequisite for the cytotoxic effects, which leads to cell death rather than being present on the extracellular level. The application of ZnO NPs for anticancer effects is supported by the cationic (positively charged) nature of the nanoparticles that induce electrostatic attraction. Hence, cationic nanoparticles exhibit greater toxicity potential toward cancer cells than their anionic or neutral counterparts as cancer cells have negatively charged phospholipids [48]. The small size and surface properties of ZnO NPs are also more selective toward cancer cells compared to that of normal cells [48]. The generation and elevation of intracellular ROS levels could evoke certain biological responses in the cancer cells attributed to induced oxidative stress. p53 deficient colon cancer cells are also deemed more susceptible to ZnO-induced cell death than p53 proficient colon cells such as HCT-116 [46]. This is due to the presence of p53 tumor-suppressive protein, which acts as a pivotal regulator which decides the biological response of the cancer cells depending on the concentration of ZnO NPs. Setyawati *et al.* [49] highlighted that reduced loading of ZnO nanomaterial induces lower oxidative stress. It then triggers the upregulation expression of anti-oxidative genes *via* the p53 pathway as a defensive mechanism for homeostatic regulation. Conversely, once the concentration of ZnO nanomaterial is beyond a threshold value, proapoptotic genes would instead be stimulated by the p53 signaling mechanism, leading to cell death [31]. In addition, ZnO NPs can also indirectly disrupt the cancer cell cycle, specifically at the proliferation stage. The reduction in the proliferation rate is even more significant in p53 proficient cells, suggesting that the putative p53 function of cell cycle arrest at G1 is triggered to limit the inheritance of cellular damage by future progeny [49].

SMEAF also reported having anticancer and antitumor properties against colon cancer. A study showed that SMEAF could induce HCT-116 colon cancer cell death by increasing oxidative stress within the cells, leading to the depletion of total glutathione (GSH), and a loss of mitochondrial potential in the cellular mitochondria [32]. Besides, SMEAF was also found to increase DNA fragmentation and induce cell cycle arrest at the G1-S transition phase [32]. In addition, another investigation further reveals that SMEAF not only depletes GSH but also induces ROS production within the HCT-116 cells. Furthermore, the elevated levels of p53 protein, caspase-3/7, caspase-9, and Bax/Bcl-2 ratio were also reported, suggesting that SMEAF acts against colon cancer cells *via* the intrinsic apoptosis pathway [31].

Therefore, to determine whether ZnO_{SMEAF} can induce increased cell death in the HCT-116 cells compared to ZnO_{Chem} and SMEAF alone, HCT-116 cells were treated with ZnO_{SMEAF} for 72 h. Similarly, the cells were treated with SMEAF and ZnO_{Chem} individually in proportion to their concentration within ZnO_{SMEAF}, as presented in Table 2. From the data obtained in Figure 8, it could be noted that the cell viability of HCT-116 is not affected by

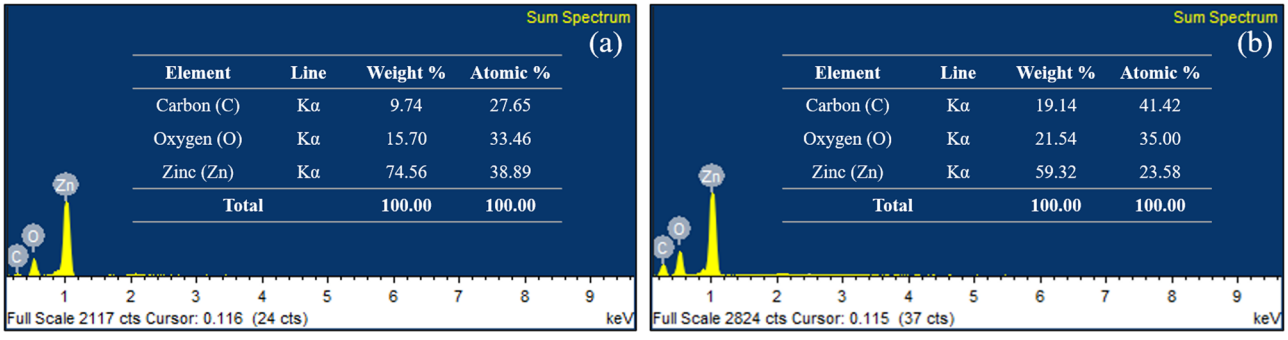

Figure 7: EDX spectra (a) ZnO_{Chem}, (b) ZnO_{SMEAF} with elemental weight and atomic distribution percentages (inset).

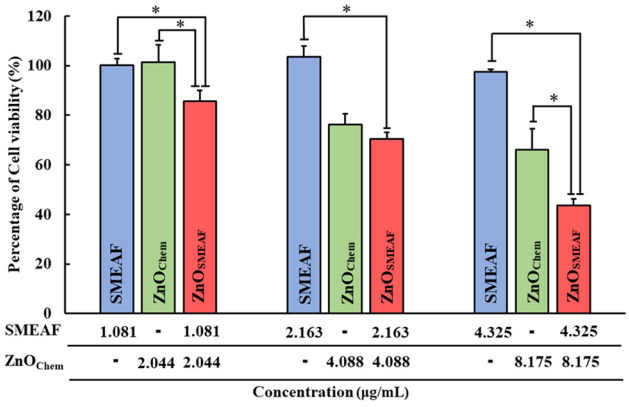

Figure 8: Cytotoxicity of SMEAF, ZnO_{Chem}, and ZnO_{SMEAF} against HCT-116. Cells were treated with each sample for 72 h before cell viability was determined using MTT assay. Error bars represent standard deviation in measurement, and a significant difference was set at $p \leq 0.05$ ($n > 3$).

the SMEAF treatment (1.081 or 2.163 µg/mL) and displayed a slight drop to 98.09 ± 1.61% when the concentration increased to 4.325 µg/mL. The obtained data on the cytotoxicity of SMEAF against HCT-116 is coherent and correlated well with the earlier findings by Goh and Kadir [32]. In their study, a decrease in the cell viability to slightly under 80% after incubating the cells with 10 µg/mL SMEAF for 72 h was observed [32]. Hence, as the concentration used in the current study is about 4.325 µg/mL, it is expected to have less cell toxicity.

On the other hand, ZnO_{Chem} induces cell death at 4.088 and 8.175 µg/mL, where the percentage of cell viability is lowered to 76.3 ± 4.37% and 66.0 ± 8.55%, respectively. The cytotoxicity displayed by ZnO_{Chem} is supported by Mohamad Sukri *et al.* [50], where the synthesized ZnO NPs using *Punica granatum* peels showed a reduction in the cell viability approximately 20% against HCT-116 cells at a concentration of 7.81 µg/mL of the biosynthesized ZnO NPs. This finding shows the competence of the biosynthesized ZnO NPs using the plant extracts, which could match those synthesized by its chemical precursors in anticancer applications.

However, when ZnO NPs are synthesized using SMEAF, ZnO_{SMEAF} displayed even significant cytotoxicity compared to treating the cells with SMEAF or ZnO_{Chem} independently. The toxicity of ZnO_{SMEAF} on HCT-116 cells increases dose-dependently, where the percentage of cell viability is reduced by 14.34 ± 4.3%, 29.49 ± 2.64%, and finally 56.36 ± 2.63% when treated with 3.125, 6.25, and 12.5 µg/mL of ZnO_{SMEAF}, respectively. Although this significant decrease in cell viability was expected at first glance, the concentration used in ZnO_{SMEAF} treatments seems to be much higher than the individual treatment of SMEAF or ZnO_{Chem}. However, the concentration of ZnO_{SMEAF} is the combined concentration of both SMEAF and ZnO_{Chem}. This is depicted in Figure 8, where it showcases how the concentration of ZnO_{SMEAF} matches up to the concentration of SMEAF and ZnO_{Chem}, creating an accurate comparison across all three types of treatment. Thus, based on the results obtained, the effectiveness of ZnO_{SMEAF} has been demonstrated in which ZnO_{SMEAF} is even more effective against HCT-116 as compared to SMEAF or ZnO_{Chem} independently, suggesting that the synthesis of ZnO NPs using SMEAF can further enhance the existing cytotoxic potential of ZnO NPs or SMEAF against colon cancer cells. To further support our claim, it was previously reported that 1 mg/mL SMEAF reduces the viability of HCT-116 cells to 75.63 ± 1.11% [31]. However, in this study, a significant drop in cancer cell viability to 85.66 ± 4.3% was observed using just 1.081 µg/mL SMEAF to aid the synthesis of ZnO NPs. On the other hand, although HCT-116 are p53 proficient cells and therefore less susceptible to ZnO-induced cell death, ZnO_{SMEAF} still managed to induce significant cell viability reduction at the relatively low loadings, suggesting its efficiency as an anti-cancer agent against HCT-116 [49]. Hence, this study demonstrates the compatibility and synergistic effect of SMEAF in the green synthesis of ZnO NP and in inducing HCT-116 cell death, and thus, a new potential treatment against colon cancer.

Subsequently, for future studies, expanding the current research through further fractionating SMEAF and in-depth exploration of its mechanism of action within colon cancer is warranted. This is better to identify the compounds responsible for their anticancer properties and shed light on the pathways it partakes in reducing cancer cell viability. As described earlier, SMEAF was previously reported to trigger cell apoptosis through the intrinsic apoptotic pathway *via* the elevation of the Bax/Bcl-2 ratio and the activation of both caspases-3/7 and 9 [31]. Thus, through a bioassay-guided fractionation approach, the efficacy of bioactive-enriched fraction(s) and/or compound(s) extracted from SMEAF can be tested on cancer cells, specifically on these effector proteins. This could also be done in conjunction with ZnO or other metallic oxide nanoparticles' biosynthesis to evaluate their effectiveness as an anticancer agent as compared to uncoupled SMEAF.

4 Conclusion

In the present work, a facile sonochemical-assisted biosynthesis of ZnO NPs using SMEAF was successfully

demonstrated. FESEM micrographs showed the nanorice shape of ZnO_{SMEAF} using ultrasound. DLS analysis evidenced that these particles have a mean particle size of 311 nm, following a normal distribution curve. XRD analysis revealed the hexagonal wurtzite structure of ZnO_{SMEAF} when the synthesis was mediated using SMEAF. FTIR spectroscopy analysis confirmed various functional groups and related compounds in the ZnO NPs and SMEAF, such as O–H, alkyl compounds, aromatic compounds, and long carbon chains of SMEAF. EDX analysis evidenced the presence of elemental carbon, oxygen, and zinc in both ZnO_{SMEAF} and ZnO_{Chem} without any impurities. In addition, the mechanism underlying the formation of biologically synthesized ZnO NPs was investigated and proposed. ZnO_{SMEAF} displayed *in vitro* cytotoxic effects against HCT-116 colon cancer cells with higher potency by MTT assay. This has reduced cell viability by 56.36 ± 2.63% at 12.5 μg/mL compared to SMEAF and ZnO NPs prepared by chemical precipitation as separate constituents. The findings of this study suggest that the ultrasonically assisted green synthesis of ZnO employing herbal plant extract could play a role in nanotechnology with biomedical applications.

Funding information: This work was supported by the Tropical Medicine and Biology Platform, School of Science and Advanced Engineering Platform, School of Engineering, Monash University Malaysia, and Xiamen University Malaysia Research Fund (XMUMRF/2019-C3/IENG/0014).

Author contributions: D.Y.S.L. and C.K.M. prepared the original draft manuscript, curated the data and results, edited revisions, and prepared manuscript visuals. JS contributed to characterization works and data curation. L.T.H.T. provided experimental resources and helped devise the experimental methodology. L.H.L., S.M., B.H.G., K.W.T., and S.Y.T. provided experimental resources and reviewed the manuscript. The study was supervised by S.Y.T. The authors applied the S.D.C. approach for the sequence of authors.

Conflict of interest: The authors state no conflict of interest.

References

[1] Khan I, Saeed K, Khan I. Nanoparticles: properties, applications and toxicities. Arab J Chem. 2019;12(7):908–31.

[2] Daniyal M, Azam A, Akhtar S. Application of nanomaterials in civil engineering. In: Khan ZH, editor. Nanomaterials and their applications. Singapore: Springer; 2018. p. 169–89.

[3] Jian W, Hui D, Lau D. Nanoengineering in biomedicine: current development and future perspectives. Nanotechnol Rev. 2020;9(1):700–15.

[4] Dejen KD, Zereffa EA, Murthy HCA, Merga A. Synthesis of ZnO and ZnO/PVA nanocomposite using aqueous Moringa Oleifeira leaf extract template: antibacterial and electrochemical activities. Rev Adv Mater Sci. 2020;59(1):464–76.

[5] Cherkasov VR, Mochalova EN, Babenyshev AV, Vasilyeva AV, Nikitin PI, Nikitin MP. Nanoparticle beacons: supersensitive smart materials with on/off-switchable affinity to biomedical targets. ACS Nano. 2020;14(2):1792–803.

[6] Kemung HM, Tan LT-H, Khaw KY, Ong YS, Chan CK, Low DYS, et al. An optimised anti-adherence and anti-biofilm assay: case study of zinc oxide nanoparticles versus MRSA biofilm. Prog Microbes Mol Biol. 2020;3(1):1–6.

[7] Pantic S, Skodric SR, Loncar Z, Pantic I. Zinc oxide nanoparticles: potential novel applications in cellular physiology, pathology, neurosciences and cancer research. Rev Adv Mater Sci. 2019;58(1):17–21.

[8] Wojnarowicz J, Chudoba T, Lojkowski W. A review of microwave synthesis of zinc oxide nanomaterials: reactants, process parameters and morphologies. Nanomaterials. 2020;10(6):1086.

[9] Khashan KS, Sulaiman GM, Hussain SA, Marzoog TR, Jabir MS. Synthesis, characterization and evaluation of anti-bacterial, anti-parasitic and anti-cancer activities of aluminum-doped zinc oxide nanoparticles. J Inorg Organomet Polym. 2020;30(9):3677–93.

[10] Khashan KS, Badr BA, Sulaiman GM, Jabir MS, Hussain SA. Antibacterial activity of zinc oxide nanostructured materials synthesis by laser ablation method. J Phys Conf Ser. 2021;1795(1):012040.

[11] Agarwal H, Venkat Kumar S, Rajeshkumar S. A review on green synthesis of zinc oxide nanoparticles – an eco-friendly approach. Resource-Efficient Tech. 2017;3(4):406–13.

[12] Singh J, Dutta T, Kim K-H, Rawat M, Samddar P, Kumar P. "Green" synthesis of metals and their oxide nanoparticles: applications for environmental remediation. J Nanobiotechnol. 2018;16(1):84.

[13] Guerriero G, Berni R, Muñoz-Sanchez AJ, Apone F, Abdel-Salam ME, Qahtan AA, et al. Production of plant secondary metabolites: examples, tips and suggestions for biotechnologists. Genes. 2018;9(6):309.

[14] Senthilkumar N, Nandhakumar E, Priya P, Soni D, Vimalan M, Vetha Potheher I. Synthesis of ZnO nanoparticles using leaf extract of Tectona grandis (L.) and their anti-bacterial, anti-arthritic, anti-oxidant and *in vitro* cytotoxicity activities. New J Chem. 2017;41(18):10347–56.

[15] Bandeira M, Giovanela M, Roesch-Ely M, Devine DM, da Silva Crespo J. Green synthesis of zinc oxide nanoparticles: a review of the synthesis methodology and mechanism of formation. Sustain Chem Pharm. 2020;15:100223.

[16] Kalpana VN, Rajeswari VD. A review on green synthesis, biomedical applications, and toxicity studies of ZnO NPs. Bioinorg Chem Appl. 2018;2018:12.

[17] Ranjbar M, Kiani M, Khakdan F. Mentha mozaffarianii mediated biogenic zinc nanoparticles target selected cancer cell lines and microbial pathogens. J Drug Deliv Sci Technol. 2020;60:102042.
[18] Godlewski MM, Kaszewski J, Kielbik P, Olszewski J, Lipinski W, Slonska-Zielonka A, et al. New generation of oxide-based nanoparticles for the applications in early cancer detection and diagnostics. Nanotechnol Rev. 2020;9(1):274–302.
[19] Cobianu C, Dumbravescu N, Serban B-C, Buiu O, Romanitan C, Comanescu F, et al. Sonochemically synthetized ZnO-graphene nanohybrids and its characterization. Rev Adv Mater Sci. 2020;59(1):176–87.
[20] Panda D, Manickam S. Cavitation technology – the future of greener extraction method: a review on the extraction of natural products and process intensification mechanism and perspectives. Appl Sci. 2019;9(4):766.
[21] Low LE, Wong SK, Tang SY, Chew CL, De Silva HA, Lee JMV, et al. Production of highly uniform pickering emulsions by novel high-intensity ultrasonic tubular reactor (HUTR). Ultrason Sonochem. 2019;54:121–8.
[22] Manickam S, Tang SY, Ashokkumar M. Development of multifunctional nanomaterials by cavitation. In: Manickam S, Ashokkumar M, editors. Cavitation: a novel energy-efficient technique for the generation of nanomaterials. Ohio, USA: CRC Press; 2014. p. 1–28.
[23] Sutariya S, Sunkesula V, Kumar R, Shah K. Emerging applications of ultrasonication and cavitation in dairy industry: a review. Cogen Food Agric. 2018;4(1):1549187.
[24] Bayrami A, Alioghli S, Rahim Pouran S, Habibi-Yangjeh A, Khataee A, Ramesh S. A facile ultrasonic-aided biosynthesis of ZnO nanoparticles using Vaccinium arctostaphylos L. leaf extract and its antidiabetic, antibacterial, and oxidative activity evaluation. Ultrason Sonochem. 2019;55:57–66.
[25] Bayrami A, Ghorbani E, Rahim Pouran S, Habibi-Yangjeh A, Khataee A, Bayrami M. Enriched zinc oxide nanoparticles by Nasturtium officinale leaf extract: joint ultrasound-microwave-facilitated synthesis, characterisation, and implementation for diabetes control and bacterial inhibition. Ultrason Sonochem. 2019;58:104613.
[26] Sayyad M, Tiang N, Kumari Y, Goh BH, Jaiswal Y, Rosli R, et al. Acute toxicity profiling of the ethyl acetate fraction of Swietenia macrophylla seeds and *in-vitro* neuroprotection studies. Saudi. Pharm J. 2017;25(2):196–205.
[27] Eid A, Elmarzugi N, El, Enshasy H. A review on the phytopharmacological effect of Swietenia macrophylla. Int J Pharm. 2013;5:47–53.
[28] Mahendra CK, Abidin SA, Htar TT, Chuah L-H, Khan SU, Ming LC, et al. Counteracting the ramifications of UVB irradiation and photoaging with Swietenia macrophylla king seed. Molecules. 2021;26(7):2000.
[29] Moghadamtousi ZS, Goh HB, Chan KC, Shabab T, Kadir AH. Biological activities and phytochemicals of Swietenia macrophylla King. Molecules. 2013;18(9):10485–63.
[30] Chen L-C, Liao H-R, Chen P-Y, Kuo W-L, Chang T-H, Sung P-J, et al. Limonoids from the seeds of Swietenia macrophylla and their anti-inflammatory activities. Molecules. 2015;20(10):18551–64.
[31] Goh BH, Chan CK, Kamarudin MNA, Abdul Kadir H. Swietenia macrophylla King induces mitochondrial-mediated apoptosis through p53 upregulation in HCT116 colorectal carcinoma cells. J Ethnopharmacol. 2014;153(2):375–85.
[32] Goh BH, Kadir H. *In vitro* cytotoxic potential of Swietenia macrophylla king seeds against human carcinoma cell lines. J Med Plant Res. 2011;5(8):1395–404.
[33] Sulaiman GM, Al-Amiery AA, Bagnati R. Theoretical, antioxidant and cytotoxic activities of caffeic acid phenethyl ester and chrysin. Int J Food Sci Nutr. 2014;65(1):101–5.
[34] Sulaiman GM. Molecular structure and anti-proliferative effect of galangin in HCT-116 cells: *in vitro* study. Food Sci Biotechnol. 2016;25(1):247–52.
[35] Jan H, Shah M, Usman H, Khan MA, Zia M, Hano C, et al. Biogenic synthesis and characterisation of antimicrobial and antiparasitic zinc oxide (ZnO) nanoparticles using aqueous extracts of the Himalayan Columbine (Aquilegia pubiflora). Front Mater. 2020;7:249.
[36] Marslin G, Siram K, Maqbool Q, Selvakesavan RK, Kruszka D, Kachlicki P, et al. Secondary metabolites in the green synthesis of metallic nanoparticles. Materials. 2018;11(6):940.
[37] Sharmila G, Thirumarimurugan M, Muthukumaran C. Green synthesis of ZnO nanoparticles using Tecoma castanifolia leaf extract: characterisation and evaluation of its antioxidant, bactericidal and anticancer activities. Microchem J. 2019;145:578–87.
[38] Basnet P, Chatterjee S. Structure-directing property and growth mechanism induced by capping agents in nanostructured ZnO during hydrothermal synthesis – a systematic review. Nano-Struct Nano-Objects. 2020;22:100426.
[39] Shah M, Fawcett D, Sharma S, Tripathy SK, Poinern GE. Green synthesis of metallic nanoparticles *via* biological entities. Materials. 2015;8(11):7278–308.
[40] Ch'ng YS, Loh YC, Tan CS, Ahmad M, Asmawi MZ, Wan Omar WM, et al. Vasodilation and antihypertensive activities of Swietenia macrophylla (Mahogany) seed extract. J Med Food. 2018;21(3):289–301.
[41] Gumaling RP, Agusan JRE, Ellacer NVCR, Abi GMT, Pajaron JRP, Joyno JRQ, et al. Increased bio-oil yield from Swietenia macrophylla seeds through microwave pretreatment and ultrasonic-assisted solvent extraction. Sustain Environ Res. 2018;28(6):430–7.
[42] Zare M, Namratha K, Thakur MS, Byrappa K. Biocompatibility assessment and photocatalytic activity of bio-hydrothermal synthesis of ZnO nanoparticles by Thymus vulgaris leaf extract. Mater Res Bull. 2019;109:49–59.
[43] Gupta M, Tomar RS, Kaushik S, Mishra RK, Sharma D. Effective antimicrobial activity of green ZnO nano particles of Catharanthus roseus. Front Microbiol. 2018;9(2030):1–13.
[44] Ch'ng YS, Tan CS, Loh YC, Ahmad M, Asmawi MZ, Yam MF. Vasorelaxation study and tri-step infrared spectroscopy analysis of Malaysian local herbs. J Pharmacopunct. 2016;19(2):145–54.
[45] Naseer M, Aslam U, Khalid B, Chen B. Green route to synthesize zinc oxide nanoparticles using leaf extracts of Cassia fistula and Melia azadarach and their antibacterial potential. Sci Rep. 2020;10(1):9055.
[46] Chung I-M, Rahuman AA, Marimuthu S, Kirthi AV, Anbarasan K, Rajakumar G. An investigation of the cytotoxicity and caspase-mediated apoptotic effect of green synthesised zinc oxide nanoparticles using Eclipta prostrata on human liver carcinoma cells. Nanomaterials. 2015;5(3):1317–30.

[47] Tanino R, Amano Y, Tong X, Sun R, Tsubata Y, Harada M, et al. Anticancer activity of ZnO nanoparticles against human small-cell lung cancer in an orthotopic mouse model. Mol Cancer Ther. 2020;19(2):502.
[48] Jasim SA, Saleh NA. The cytotoxic effect of zinc oxide on colon cancer cell lines *in vitro*. Indian J Public Health Res Dev. 2019;10(10):1–5.
[49] Setyawati MI, Tay CY, Leong DT. Effect of zinc oxide nanomaterials-induced oxidative stress on the p53 pathway. Biomaterials. 2013;34(38):10133–42.
[50] Mohamad Sukri SNA, Shameli K, Mei-Theng Wong M, Teow S-Y, Chew J, Ismail NA. Cytotoxicity and antibacterial activities of plant-mediated synthesised zinc oxide (ZnO) nanoparticles using Punica granatum (pomegranate) fruit peels extract. J Mol Struct. 2019;1189:57–65.